PHOTONICS Research

Antimonene: a long-term stable two-dimensional saturable absorption material under ambient conditions for the mid-infrared spectral region

Hongyu Luo,[1,†] Xiangling Tian,[2,†] Ying Gao,[1] Rongfei Wei,[3] Jianfeng Li,[1,5] Jianrong Qiu,[2,4,6] and Yong Liu[1]

[1]State Key Laboratory of Electronic Thin Films and Integrated Devices, School of Optoelectronic Science and Engineering, University of Electronic Science and Technology of China (UESTC), Chengdu 610054, China
[2]State Key Laboratory of Luminescent Materials and Devices and School of Materials Science and Engineering, South China University of Technology, Guangzhou 510641, China
[3]Department of Physics, Zhejiang Normal University, Jinhua 321004, China
[4]State Key Laboratory of Modern Optical Instrumentation, College of Materials Science and Engineering, Zhejiang University, Hangzhou 310027, China
[5]e-mail: lijianfeng@uestc.edu.cn
[6]e-mail: qjr@zju.edu.cn

Received 5 June 2018; revised 19 July 2018; accepted 20 July 2018; posted 23 July 2018 (Doc. ID 334079); published 23 August 2018

We experimentally demonstrate a long-term stable two-dimensional saturable absorption material under ambient conditions—multi-layer antimonene feasible for the mid-infrared spectral region—for the first time to our knowledge. The multi-layer antimonene material prepared using a liquid-phase exfoliation method was coated on a quartz/CaF_2 for characterizations and an Au mirror as a reflection-type saturable absorber (SA) device. It has a modulation depth of 10.5%, a saturation peak intensity of 0.26 GW/cm^2, and a non-saturation loss of 19.1% measured at 2868.0 nm using the typical power-dependent method. By introducing the SA device into a linear-cavity Ho^{3+}/Pr^{3+}-codoped fluoride fiber laser at 2865.0 nm, stable *Q*-switched pulses were obtained. It generated a maximum output power of 112.3 mW and pulse energy of 0.72 μJ, while the shortest pulse duration and largest repetition rate were 1.74 μs and 156.2 kHz, respectively. The long-term stability of the SA device was also checked using the same laser setup within 28 days. The results indicate that multi-layer antimonene is a type of promising long-term stable SA material under ambient conditions that can be applied in the mid-infrared spectral region.

OCIS codes: (140.3070) Infrared and far-infrared lasers; (140.3510) Lasers, fiber; (140.3540) Lasers, Q-switched; (160.4236) Nanomaterials.

https://doi.org/10.1364/PRJ.6.000900

1. INTRODUCTION

Pulsed fiber lasers in the 3 μm mid-infrared region are currently promising sources for longer-wavelength mid-infrared emissions by means such as optical parametric oscillators [1], stimulated Raman scattering (SRS) [2], supercontinuum (SC) generation [3], and soliton self-frequency shift (SSFS) [4]. Moreover, such lasers have quite large potential in medical surgery for cutting/ablating tissues containing water [5–7] and specific material processing [8] owing to the high overlapping of the output spectral region with the strong water (or OH bond) absorption band.

Saturable absorbers (SAs), as the core devices for pulse generation by passive *Q*-switching or mode-locking, have been well developed. Different from mode-locking, which has a femtosecond (fs) to picosecond (ps) temporal duration [9,10] commonly with a quite high peak power [10], *Q*-switching can usually give a larger pulse energy with a longer pulse duration of nanoseconds (ns) to microseconds (μs) and a moderate peak power [11]. This technique more easily avoids some nonlinear effects that are undesired for some cases. For example, when scaling pulse output based on a master oscillator power amplifier (MOPA) for only higher average power and energy, a too-high peak power will lead to spectrum broadening, thus reducing spectrum density. Moreover, *Q*-switching is also more favored by laser surgery as a result of its sufficiently energetic and powerful output [12,13].

Until now, different SAs have been applied in *Q*-switched fiber lasers around 3 μm [14–24]. Semiconductor saturable absorber mirrors (SESAMs), as one of the most mature SAs, have been confirmed to be a reliable *Q*-switcher in this spectral region [14,15]. Despite their high stability and flexibly controllable parameters, the narrow operation bandwidth [typically

hundreds of nanometers (nm)] and typically longest effective wavelength of 3.2 μm limit its further applications at longer wavelengths within the mid-infrared region. Fe^{2+}:ZnSn crystal is another mature mid-infrared SA that has a relatively broad mid-infrared absorption range of 2.5–4.2 μm. It has been also used to *Q*-switch fiber lasers around 3 μm, especially for high power conditions [16,17], resulting from its high damage threshold. However, the bulk nature blocks its development toward all-fiber SA devices. Recently, the fabrication of Fe^{2+}:ZnSn nanocrystals [18] has unlocked its potential in an all-fiber scheme.

In the past decade, two-dimensional (2D) materials, a new family of materials, have attracted a large amount of attention in the fields of condensed matter physics, material science, nanotechnology, chemistry, and optoelectronics, owing to their extraordinary properties. Because of their broadband saturable absorption and nonlinear optical properties, they are regarded as the most promising candidates for broadband SAs. Graphene, as the first discovered 2D material in 2004 [25], was first applied in pulse generation in an Er^{3+}-doped fiber laser at 1.55 μm in 2009 [26]. In 2013, its ability of *Q*-switching in the 3 μm region was demonstrated first in an Er^{3+}-doped fluoride fiber laser [19]. However, its low modulation depth resulted from the low absorption efficiency (2.3% per layer), making it not very suitable for short *Q*-switching. After that, some other 2D materials (e.g., topological insulators (TIs) [20] and transition-metal dichalcogenides (TMDs) [21,22]) were found and used to *Q*-switch Ho^{3+}- or Er^{3+}-doped fluoride fiber lasers to generate pulses around 3 μm. Although TIs can provide a large modulation depth in a broad band, they possess the drawback of a complex preparation process as a result of compound with two different elements. Moreover, the band gaps of TMDs are so naturally large that they are unavailable for the mid-infrared region, although they can be reduced to the level available for mid-infrared application by introducing a series of defects, which complicates the preparation. Recently, black phosphorus (BP), a 2D material composed by Group-V elements, began to attract our attention. Different from the other 2D materials mentioned above, BP has a unique direct band gap, which is dependent on the number of layers [27]. Specifically, its band gap can be tuned from ~0.3 eV (bulk) to ~2 eV (monolayer) flexibly by changing the layer number and hence filling up the gap between the zero band gap of graphene and the large band gaps of TMDs. This feature makes it very useful for optoelectronic applications, especially in the near- and mid-infrared spectral regions. Recently, passively *Q*-switched Er^{3+}-doped and Ho^{3+}/Pr^{3+}-codoped fluoride fiber lasers at around 3 μm using multi-layer BP as SAs were demonstrated [23,24]. However, BP is quite unstable due to its ease of oxidation under ambient conditions, and it may degrade within hours, especially for monolayer or few-layer samples. This oxidation would be further accelerated under thermal effects in the existence of water and oxygen [23]. This defect limits its application to a great extent. Although several strategies have been proposed in order to enhance its anti-oxidation ability, these methods may complicate the fabrication process while introducing unwanted defects or scattering loss [28]. Therefore, people have started to search for other Group-V materials with high stability.

Among them, antimonene has been noticed, owing to its high stability [29] and some other outstanding merits such as high carrier mobility [30], excellent thermal conductivity [31], strain-induced band transition [32,33], and broadband absorption [34]. Although monolayer antimonene is a semiconductor with a large indirect band gap of 2.28 eV, the band gap can theoretically decrease to 0 with the increase of the number of layers [32], thus expanding its available absorption band for the mid-infrared spectral region. Recently, Song *et al.* experimentally characterized the nonlinear absorption of few-layer antimonene at 800 nm and 1500 nm while showing its potential as an SA for pulse generation (by *Q*-switching and mode-locking) in an Er^{3+}-doped silica fiber laser at 1.55 μm for the first time [28], which opens the door to research on antimony nanosheet SA. Very recently, Wang *et al.* presented a *Q*-switched Nd:YAG laser at 946 nm and 1064 nm and a *Q*-switched Nd:YVO_4 laser at 1342 nm using multi-layer antimonene SA [35]. These efforts were deployed in the near-infrared spectral region; however, there is no report yet on the study of its saturable absorption property and potential as an SA in the mid-infrared region beyond 2 μm to the best of our knowledge.

In this paper, we report on the fabrication of a multi-layer antimonene sample using a liquid-phase exfoliation (LPE) method, while revealing its saturable absorption property and potential as an SA in pulse generation in the 3 μm region, for the first time to our knowledge. By introducing the multi-layer antimonene-coated Au mirror SA into a linear-cavity Ho^{3+}/Pr^{3+}-codoped fluoride fiber laser at ~2.87 μm, stable *Q*-switched pulses were obtained. The pulse outputs [e.g., output power, pulse energy, pulse duration, repetition rate, and optical and radio frequency (RF) spectra] were all characterized. The long-term stability of the SA within 28 days was also checked. The results indicate that multi-layer antimonene is a type of promising long-term stable SA under ambient conditions for the mid-infrared spectral region.

2. PREPARATION AND CHARACTERIZATIONS OF A MULTI-LAYER ANTIMONENE SA

The multi-layer antimonene material used in our experiment was prepared using the LPE method. Bulk antimony with high purity (99.999%) was ground first. Then, the antimony powder was immersed into N-methyl-2-pyrrolidon (NMP) to experience ultrasonication for several hours (several consecutive 0.5 h with a 0.5-h recess between two adjacent 0.5 h) to form the liquid dispersion. Finally, the stable multi-layer antimonene dispersion was collected from the supernatant after centrifugation to remove the un-exfoliated bulk matrix at 2000 r/min for 30 min, as shown in Fig. 1(a). For different characterizations, a few same-volume droplets of the dispersion were coated onto a quartz substrate [for transmission electron microscopy (TEM), atomic force microscopy (AFM), Raman spectrum and X-ray photoemission spectroscopy (XPS) measurements], a CaF_2 substrate (for nonlinear absorption measurement), and an Au mirror (as the SA), as shown in Fig. 1(b). Then these samples were dried in a vacuum oven with the addition of the appropriate amount of ethanol to accelerate the volatilization of the NMP.

Figures 2(a) and 2(b) show the TEM images of the multi-layer antimonene sample measured using a JEOL JEM-2100F

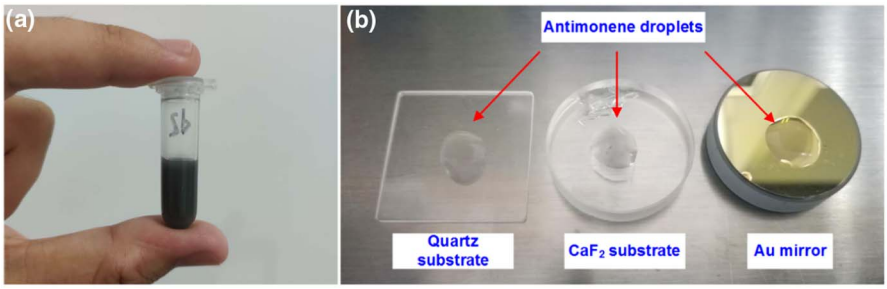

Fig. 1. Images of (a) multi-layer antimonene dispersion and (b) multi-layer antimonene droplets on quartz substrate, CaF_2 substrate, and Au mirror (from left to right).

microscope operated at 200 kV. The low-magnification TEM image as displayed in Fig. 2(a) reveals that the lateral of the multi-layer antimonene is in the range of 0.5–1.0 μm. The high-resolution TEM image, as displayed in Fig. 2(b), shows that the lattice distance is about 0.31 nm, corresponding to the (0, 1, 2) lattice plane. The measured AFM (Nanoscope Multi Mode V, Digital Instruments/Bruker Systems) was used to characterize the thickness of the multi-layer antimonene sample. Figures 2(c) and 2(d) show a typical AFM image and the relative height profile, respectively. It is seen that the average thickness is about 35.3 nm, corresponding to about 88 layers [36], which has a stronger interaction with light than a few-layer or monolayer one [37,38]. Note that more layers or less layers with a <0.4 eV (~3 μm) bandgap sample were also available for our current system in principle. The Raman spectrum of the multi-layer antimonene sample was also measured using a

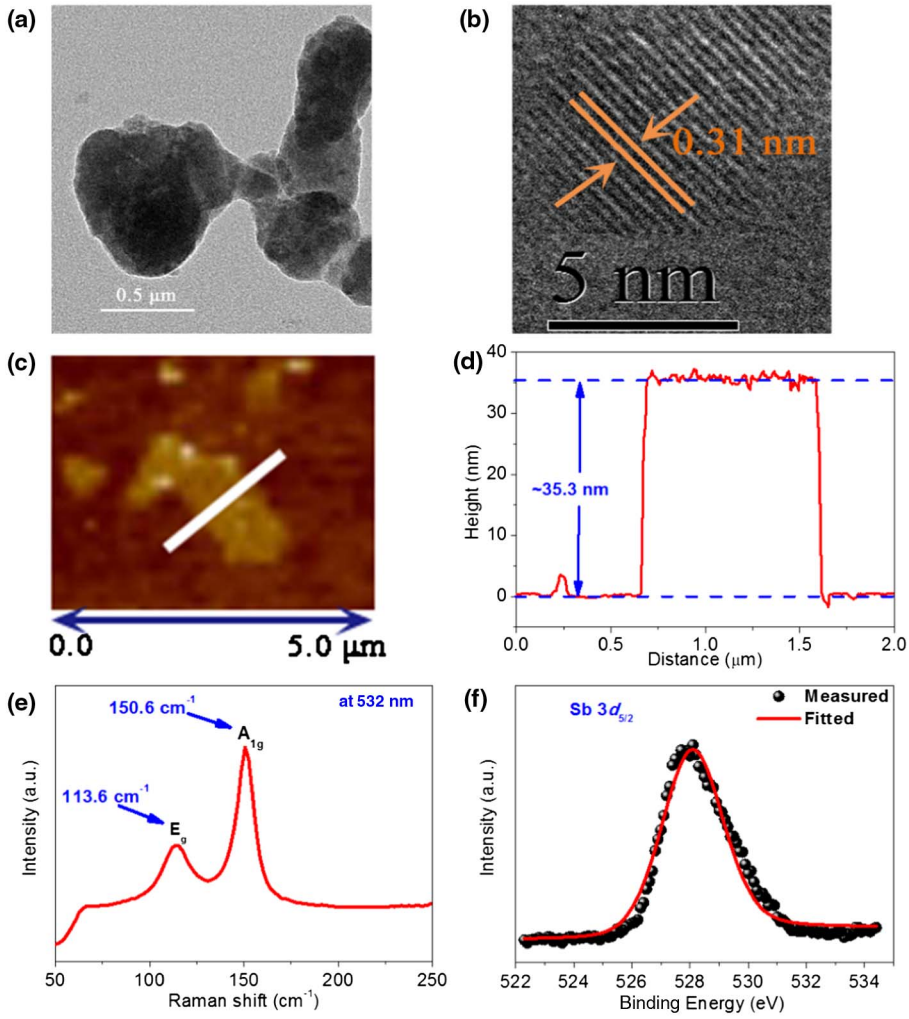

Fig. 2. Material characterizations of the multi-layer antimonene sample: (a) low- and (b) high-magnification TEM images; (c) AFM image and (d) the corresponding height profile; (e) Raman and (f) XPS spectra.

confocal microscopy system (RenishaiwnVia, Gloucestershire, UK) excited at 532 nm at room temperature, as shown in Fig. 2(e). Two typical sharp scattering peaks (i.e., E_g and A_{1g}) were observed, in which the former, originating from an in-plane vibrational mode, is located at 113.6 cm^{-1}, and the latter, originating from an out-of-plane vibrational mode, is located at 150.6 cm^{-1}; this is basically consistent with the results of 31.6 nm thick multi-layer antimonene measured by Lu *et al.* [39]. Besides, the Raman peak frequencies also matched well with the thickness previously measured by AFM considering the relation between E_g and A_{1g} peak frequencies and multi-layer antimonene sample thickness revealed by Ji *et al.* [36]. Figure 2(f) shows the XPS measured using an X-ray photoemission spectroscopy system (K-Alpha, Thermo Science, UK) in order to detect the chemical states of the multi-layer antimonene sample. It is seen that there is a sharp symmetric photoelectron peak, which describes Sb-Sb $^3d_{5/2}$ orbital bonding at 528 eV. Note that there is only a mono-peak in the XPS spectrum, indicating the non-existence feature and the stability of the sample [39].

To reveal the nonlinear absorption of the multi-layer antimonene sample at ~3 μm, a typical power-dependent measurement setup involving a balance twin-detector arrangement was built up as shown in Fig. 3(a). The laser source is a self-built SESAM passively mode-locked Ho^{3+}/Pr^{3+}-codoped fluoride fiber laser that has a similar structure to that in Ref. [9]. It gave a center wavelength of 2868.0 nm, a pulse duration of ~20 ps, and a repetition rate of 17.86 MHz. A band-pass filter (FB3000-500, Thorlabs) was placed along the light path to remove the residual 1150 nm pump laser. After that, an Au mirror was used to steer the light along the optical table. A beam splitter was placed at an angle of 45° with respect to the light path, which had a measured transmittance/reflectance ratio of 55:45 at 2868.0 nm. The transmitted laser was focused using a 20 mm focal length uncoated CaF_2 plano-convex lens (LA5315, Thorlabs) and then went through the multi-layer antimonene-coated CaF_2 substrate prepared earlier. A power meter detector (Detector 1) was placed after it to record the power, P_1. The reflected laser was focused using another similar CaF_2 lens and then went through a clean CaF_2 substrate. Another power meter detector (Detector 2) was placed after it to record the power, P_2, as the reference. In this scheme, the multi-layer antimonene-coated CaF_2 substrate was held by a mount fixed with a one-dimensional translation stage. In order to find the focused point of the CaF_2 plano-convex lens where the beam has an about 10 μm diameter estimated according to the parameters of the used CaF_2 lenses and Ho^{3+}/Pr^{3+}-codoped fluoride fiber, the multi-layer antimonene-coated CaF_2 substrate was adjusted along the axis of the light path to maximize P_1 at an appropriate output power. The transmittance of the multi-layer antimonene sample could be calculated by $45P_1/55P_2$. At various laser powers, the transmittances were recorded. Figure 3(b) shows the transmittance as a function of the pulse peak intensity. The relative parameters of the multi-layer antimonene sample were obtained by fitting using the following formula:

$$T(I) = 1 - \Delta T \cdot \exp(-I/I_{sat}) - T_{ns}, \quad (1)$$

where $T(I)$ is the transmittance, ΔT is the modulation depth, I_{sat} is the saturation peak intensity, and T_{ns} is the non-saturation loss. Finally, ΔT, I_{sat}, and T_{ns} were fitted to be 10.5%, 0.26 GW/cm^2, and 19.1%, respectively.

3. EXPERIMENTAL DESIGN OF *Q*-SWITCHED FIBER LASER

The experimental setup of the passively *Q*-switched Ho^{3+}/Pr^{3+}-codoped fluoride fiber laser using multi-layer antimonene as the SA is shown in Fig. 4. In this arrangement, two commercially available laser diodes (LDs) (Eagleyard Photonics, Berlin) around 1150 nm were used to pump the gain fiber after polarization multiplexing through a polarized beam splitter (PBS) and then focusing by an uncoated CaF_2 plano-convex lens (LA5315, Thorlabs) with a 20 mm focal length. This lens also functions as the collimator of the laser out-coupled from the gain fiber core. A specifically designed dichroic mirror with a ~96% transmittance around 1150 nm and a >95% reflectance around 3 μm was placed between the PBS and CaF_2 lens at an angle of 30° with respect to the pump beam to steer the laser. A 3 μm band-pass filter (FB3000-500, Thorlabas) with a full width at half-maximum (FWHM) of 500 nm was used to block the residual pump. It had a measured transmittance of ~76% at ~2.87 μm. The gain fiber (Fiberlabs, Japan) was a piece of commercial double-cladding Ho^{3+}/Pr^{3+}-codoped fluoride fiber, with an octangular pump

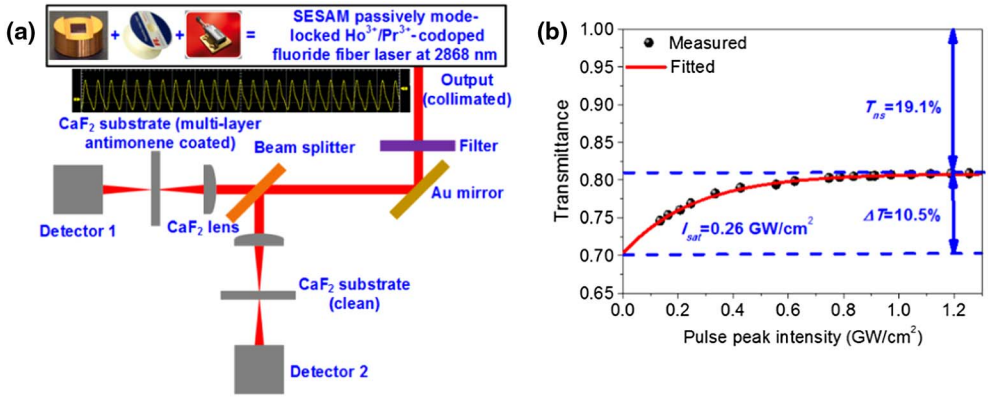

Fig. 3. (a) Experimental setup of nonlinear absorption measurement at 2868.0 nm. (b) Transmittance of the multi-layer antimonene sample as a function of pulse peak intensity.

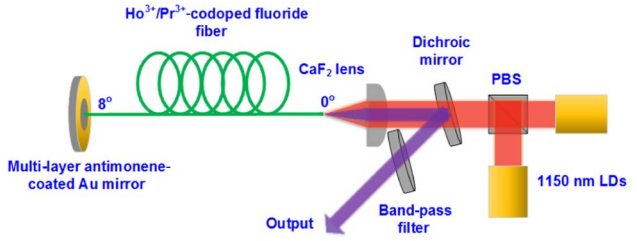

Fig. 4. Experiment setup of passively Q-switched Ho^{3+}/Pr^{3+}-codoped fluoride fiber laser using multi-layer antimonene as the SA.

core with a diameter of 125 μm and a numerical aperture (NA) of 0.5 and a circular core with a diameter of 10 μm and an NA of 0.2. The concentration of the Ho^{3+} and Pr^{3+} were 30,000 and 2500 ppm, respectively. Note that the pump was launched into the inner cladding of the gain fiber. The launching efficiency was measured to be 82% using a piece of short Ho^{3+}/Pr^{3+}-codoped fluoride fiber with the same size. The fiber length of 5.2 m could provide a measured ~90% pump absorption efficiency. The fiber end close to the pump was perpendicularly cleaved as one cavity feedback and the output coupler with the help of 4% Fresnel reflection. The other end of the fiber was cleaved at an angle of 8° to avoid parasitic lasing. The multi-layer antimonene-material-coated Au mirror was placed against the angle cleaved fiber end, acting as the SA, and terminated cavity. The Au mirror was held by a high-precision differential mirror mount. An InAs detector with a response time of 2 ns connected with a 500 MHz bandwidth digital oscilloscope was used to capture temporal pulse trains and waveforms. An RF spectrum analyzer (AV4033A) with a scanning range of 30 Hz–18 GHz was used to measure the pulsed RF spectrum. A monochromator with a scanning resolution of 0.1 nm (Princeton Instruments Acton SP2300) was utilized to measure the optical spectrum.

4. Q-SWITCHED RESULTS

A continuous-wave (CW) laser was first generated at a low launched pump power of 30.5 mW, which mainly contributed to the compact backward-pumped cavity scheme and efficient gain fiber. With the launched pump power increasing to 93.3 mW, a stable Q-switching regime with a low amplitude fluctuation of ±3% was obtained. The pulse train and single pulse waveform at this pump level were captured as shown in Fig. 5(a) and its inset, respectively. The repetition rate and pulse duration were 59.52 kHz and 4 μs, respectively. Further increasing the pump power, the laser was always operated in a stable Q-switching regime until the launched pump power of 489.0 mW, as shown in Fig. 5(c), yielding a repetition rate of 156.2 kHz and a pulse duration of 1.97 μs. At the middle launched pump power of 358.6 mW, the pulsed temporal behavior was also captured as an example, as shown in Fig. 5(b), giving a repetition rate of 119 kHz and a pulse duration of 1.74 μs. Once the launched pump power was adjusted beyond 489.0 mW, the pulse train exhibited strongly increased repetition rate and decreased amplitudes, and then was transformed to CW with the slightly further increased launched pump power of 498.2 mW. At this time, if the launched pump power was adjusted back to the level around 489.0 mW, a stable Q-switching regime was observed again with almost the same repetition rate and pulse duration as before, indicating that the multi-layer antimonene material was free from damage. At this pump level, the influence on the SA was estimated to be

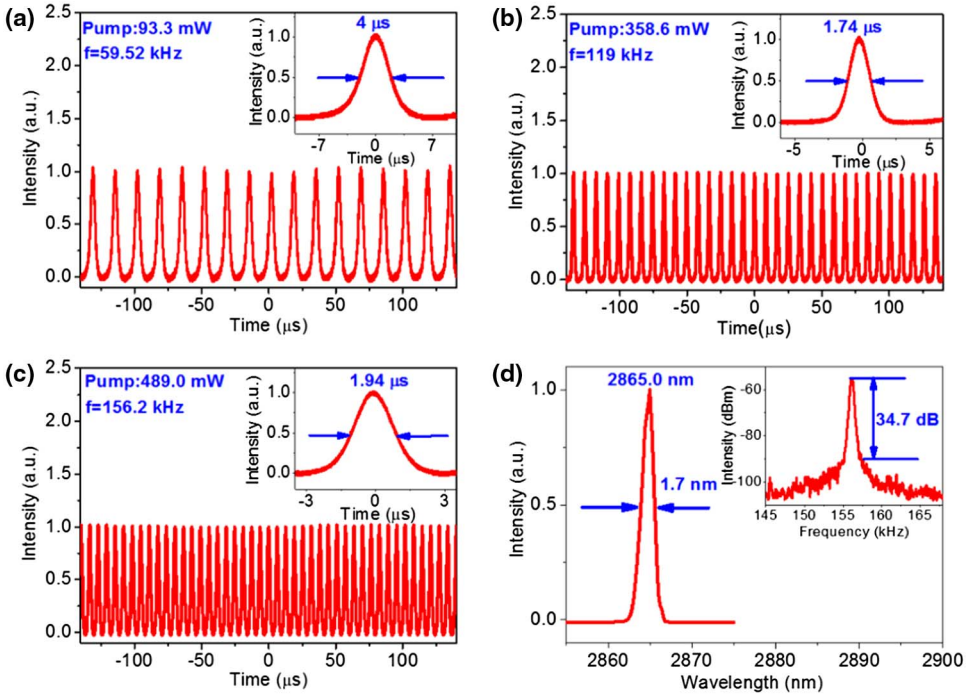

Fig. 5. Q-switched trains and single pulse waveforms (insets) at the launched pump power of (a) 93.3 mW, (b) 358.6 mW, and (c) 489.0 mW. (d) Q-switched optical and RF (inset) spectra at the launched pump power of 489.0 mW.

0.95 J/cm^2 according to the fiber size and Q-switched pulse parameters. The disappearance of Q-switching was due mainly to the temporary failure of the SA under excessive heat from the Q-switched signal laser and ~10% residual pump, which has been observed in passively Q-switched fiber lasers at this band based on other nonlinear materials as well [21,40]. If the launched pump power was increased to beyond ~1.5 W, corresponding to an output power of ~340 mW, however, it became difficult to obtain further Q-switching by decreasing the launched pump power to below 489.0 mW, due to the permanent damage of the multi-layer antimonene material under heat from such a high power. Before its damage, the optical and RF spectra of the stable Q-switched pulses at the launched pump of 489.0 mW were measured as shown in Fig. 5(d) and its inset, respectively. The center wavelength and FWHM were 2865.0 nm and 1.7 nm, respectively. The signal-to-noise ratio (SNR) of 34.7 dB was also located at the typical range of passively Q-switched fiber lasers. The peak frequency of 156.2 kHz was in accordance with the repetition rate.

In the stable Q-switched pump range of 93.3–489.0 mW, the output characteristics including pulse duration, repetition rate, output power, and pulse energy with the varied launched pump power were all measured/calculated. Figure 6(a) shows the pulse duration and repetition rate as a function of the launched pump power. It is seen that the pulse duration decreases first from 4 to 1.74 μs monotonously with the increased launched pump from 93.3 to 358.6 mW. Then, it increased from 1.74 to 1.96 μs with the further increased launched pump power of 489.0 mW, which may result from excessive heat-induced performance changes of the multi-layer antimonene material. This is an indicator of the disappearing Q-switching with further increased pump power. The shortest pulse duration of 1.74 μs also matched well with the theoretical limitation calculated using the following formula [41]:

$$\tau = 1.76\frac{2T_R}{\Delta R}, \tag{2}$$

where τ is the shortest pulse duration, T_R is the cavity round-trip time, and ΔR is the modulation depth. In our case, the cavity round-trip time was 0.0513 μs where the cavity length was 5.2 m, the fiber refractive index at 2.87 μm was set as 1.48, the speed of light was 3×10^8 m/s, and ΔR was equal to ΔT, i.e., 10.5%, measured earlier. Finally, τ was calculated to be 1.72 μs. The repetition rate increased monotonously from 59.52 to 156.2 kHz with the increased pump power in this range as a result of faster population accumulation on the laser's upper level after one pulse formation. Figure 6(b) shows the Q-switched output power and calculated pulse energy with the varied launched pump power. The output power increased almost linearly at a slope efficiency of 24.7% with respect to the launched pump power. This was also the highest level from a passively Q-switched fiber laser using 2D materials in the 3 μm region, which can be mainly attributed to the low insertion loss of the SA and efficient cavity design. The pulse energy increased linearly first and then tended to saturate. At the launched pump power of 489.0 mW, the maximum output power of 112.3 mW and pulse energy of 0.72 μJ were obtained. To confirm that the Q-switched operation was caused by the multi-layer antimonene material, the micrometer (μm)-pumped fiber end was removed onto the clean zone of the Au mirror. No Q-switching signs were seen except some occasional relaxation oscillation signals with low amplitudes, no matter how the position of the Au mirror was adjusted and how the pump power changed, indicating that the Q-switched pulses were indeed induced by the multi-layer antimonene material.

To evaluate the stability of our multi-layer antimonene sample, we repeated the Q-switched laser experiment described above 2 days before our submission of this paper. Since the built-up laser arrangement was almost kept unchanged after the experiment was finished 28 days ago, it should have a great repeatability if the performance of the SA was stable enough. As a result, stable Q-switched pulses were still achieved by adjusting the positon of the SA, although the variation ranges of repetition rate, pulse duration, output power, and pulse energy with the pump power were a little different. Also, the power stability of the Q-switched operation at the launched pump power of ~480 mW was characterized within 10 h as shown in Fig. 7. The low calculated root mean square (RMS) fluctuations of about 0.54% indicated its stable performance. Note that the SA sample was stored in the atmosphere only with an unsealed cover on it to avoid dust pollution in the past four weeks. This was a sharp contrast with our previously reported passively Q-switched Ho^{3+}-doped and mode-locked Ho^{3+}/Pr^{3+}-codoped fluoride fiber lasers in this region using multi-layer BP as the SA [24], in which there were only about 3 days for the used BP sample before failure for pulse generation under ambient conditions. The results indicate that multi-layer antimonene is a type of long-term stable SA material under ambient conditions for the mid-infrared spectral region.

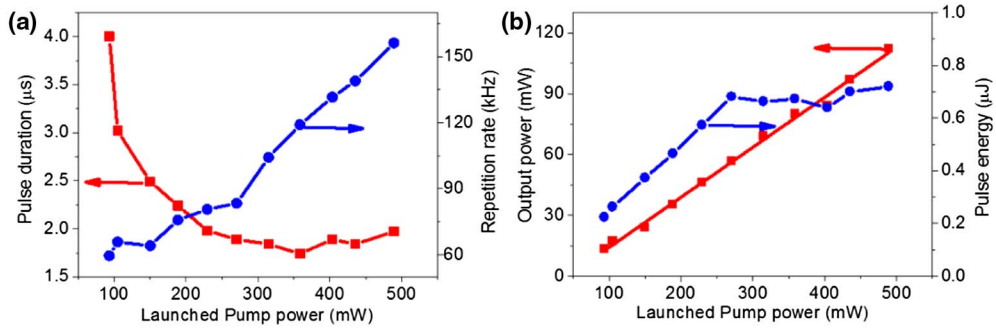

Fig. 6. (a) Pulse duration and repetition rate and (b) output power and pulse energy as functions of the launched pump power.

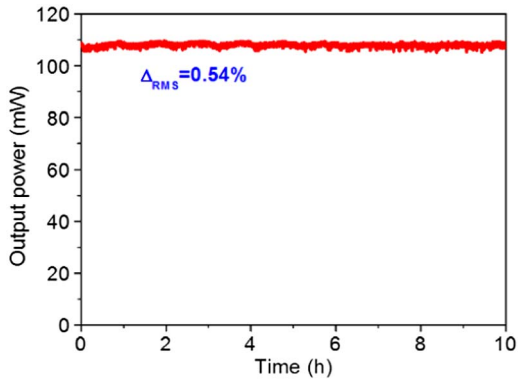

Fig. 7. Evolution of Q-switched output power within 10 h at the launched pump power of ~480 mW.

5. CONCLUSION

In summary, we experimentally confirm multi-layer antimonene as a long-term stable SA material under ambient conditions for the mid-infrared spectral region, for the first time to our knowledge. Using the widely used LPE method, a multi-layer antimonene sample was prepared and characterized by TEM, AFM, Raman spectrum, and XPS measurements. Its saturable absorption property at 2868.0 nm was studied using the typical power-dependent measurement method. A modulation depth of 10.5%, saturation peak intensity of 0.26 GW/cm^2, and non-saturation loss of 19.1% were achieved. Using multi-layer antimonene as the SA, a passively Q-switched Ho^{3+}/Pr^{3+}-codoped fluoride fiber laser at 2865.0 nm was realized. A maximum output power of 112.3 mW at a slope efficiency of 24.7% and a pulse energy of 0.72 μJ was achieved. The largest repetition rate and shortest pulse duration was 156.2 kHz and 1.74 μs, respectively. Moreover, the long-term stability of the multi-layer antimonene SA under ambient conditions was also checked after four weeks. The results indicate that multi-layer antimonene is a promising long-term stable SA material under ambient conditions for the mid-infrared region. In our case, further output scaling of Q-switching was terminated by CW oscillation, resulting from excessive heat-induced SA failure. This meant that heat control was very critical for the multi-layer antimonene SA to realize higher power and energy. In the next step, a special water cooling system for this type of material-coated Au mirror SA device could be designed to accelerate the heat dissipation. Besides, the laser spot onto the SA could be carefully controlled using a pair of suitable lenses to reduce the intensity, hence enhancing the power damage threshold.

Considering the ultrafast recovery time of multi-layer antimonene material, mode-locking should be also feasible for the mid-infrared spectral region in principle. However, no CW mode-locking was observed in our case no matter how the SA and pump power were adjusted, indicating that the well-known CW mode-locking condition was never satisfied, as described as the following inequation [42]:

$$E_p > E_{\mathrm{sat},L} E_{\mathrm{sat},A} \Delta R, \tag{3}$$

where E_p is the intra-cavity pulse energy, $E_{\mathrm{sat},L}$ and $E_{\mathrm{sat},A}$ are the saturation energies of the gain fiber and SA, respectively, and ΔR is the modulation depth. In the future, more attempts at mode-locking could be made to exploit its potential in ultrafast pulse generation. Few-layer animonene with lower modulation depth and higher uniformity combined with an optimized ring cavity with a higher intra-cavity pulse energy was planned, which could make the inequation above satisfied more easily. Furthermore, as a broadband SA material, multi-layer antimonene has large potential in Q-switching/mode-locking at longer wavelengths in the mid-infrared spectral region as well, which is another future research direction.

Funding. National Natural Science Foundation of China (NSFC) (61722503, 61435003, 61421002); Open Fund of Science and Technology on Solid-State Laser Laboratory; Fundamental Research Funds for the Central Universities (ZYGX2016J068); International Scientific Cooperation Project of Sichuan Province (2017HH0046); National Key R&D Program of China (YS2018YFB110012); Natural Science Foundation of Zhejiang Province (LQ18A040004).

†These authors contributed equally to this work.

REFERENCES

1. T. H. Allik, S. Chandra, D. M. Rines, P. G. Schunemann, J. A. Hutchinson, and R. Utano, "Tunable 7-12-μm optical parametric oscillator using a Cr, Er:YSGG laser to pump CdSe and $ZnGeP_2$ crystals," Opt. Lett. **22**, 597–599 (1997).
2. M. Bernier, V. Fortin, M. El-Amraoui, Y. Messaddeq, and R. Vallée, "3.77 μm fiber laser based on cascaded Raman gain in a chalcogenide glass fiber," Opt. Lett. **39**, 2052–2055 (2014).
3. J. Gauthier, V. Fortin, J. Carrée, S. Poulain, M. Poulain, R. Vallée, and M. Bernier, "Mid-IR supercontinuum from 2.4 to 5.4 μm in a low-loss fluoroindate fiber," Opt. Lett. **41**, 1756–1759 (2016).
4. S. Duval, J. Gauthier, L. Robichaud, P. Paradis, M. Olivier, V. Fortin, M. Bernier, M. Piché, and R. Vallée, "Watt-level fiber-based femtosecond laser source tunable from 2.8 to 3.6 μm," Opt. Lett. **41**, 5294–5297 (2016).
5. R. Kaufmann and R. Hisbst, "Pulsed 2.94 μm erbium–YAG laser skin ablation—experimental results and first clinical application," Clin. Exp. Dermatol. **15**, 389–393 (1990).
6. J. T. Walsh and T. F. Deutsch, "Er:YAG laser ablation of tissue: measurement of ablation rates," Lasers Surg. Med. **9**, 208–211 (1989).
7. R. Kaufmann, A. Hartmann, and R. Hibst, "Cutting and skin-ablative properties of pulsed mid-infrared laser surgery," J. Dermatol. Surg. Oncol. **20**, 112–118 (1994).
8. R. Ostrowski, J. Marcak, A. Rycyk, M. Strelec, I. Smelter, and A. Koss, "Er:YAG laser system for cleaning of painted surfaces," in *Conference on Lasers and Electro-Optics Europe*, Munich, Germany (2006), p. 676.
9. J. F. Li, D. D. Hudson, Y. Liu, and S. D. Jackson, "Efficient 2.87 μm fiber laser passively switched using a semiconductor saturable absorber mirror," Opt. Lett. **37**, 3747–3749 (2012).
10. S. Antipov, D. D. Hudson, A. Fuerbach, and S. D. Jackson, "High-power mid-infrared femtosecond fiber laser in the water vapor transmission window," Optica **3**, 1373–1376 (2016).
11. S. Tokita, M. Murakami, S. Shimizu, M. Hashida, and S. Sakabe, "12 W Q-switched Er:ZBLAN fiber laser at 2.8 μm," Opt. Lett. **36**, 2812–2814 (2011).
12. A. Zajac, M. Skorczakowski, J. Swiderski, and P. Nyga, "Electrooptically Q-switched mid-infrared Er:YAG laser for medical applications," Opt. Express **12**, 5125–5130 (2014).
13. M. Skorczakowski, J. Swiderski, W. Pichola, P. Nyga, A. Zajac, M. Maciejewska, L. Galecki, J. Kasprzak, S. Gross, and A. Heinrich, "Mid-infrared Q-switched Er:YAG laser for medical applications," Laser Phys. Lett. **7**, 498–504 (2010).

14. J. F. Li, H. Y. Luo, Y. L. He, Y. Liu, L. Zhang, K. M. Zhou, A. G. Rozhin, and S. K. Turistyn, "Semiconductor saturable absorber mirror passively Q-switched 2.97 μm fluoride fiber laser," Laser Phys. Lett. **11**, 065102 (2014).
15. H. Y. Luo, J. F. Li, J. T. Xie, B. Zhai, C. Wei, and Y. Liu, "High average power and energy microsecond pulse generation from an erbium-doped fluoride fiber MOPA system," Opt. Express **24**, 29022–29032 (2016).
16. T. Zhang, G. Y. Feng, H. Zhang, S. G. Ning, B. Lan, and S. H. Zhou, "Compact watt-level passively Q-switched ZrF_4-BaF_2-LaF_3-AlF_3-NaF fiber laser at 2.8 μm using Fe^{2+}:ZnSe saturable absorber mirror," Opt. Eng. **55**, 086106 (2016).
17. C. Wei, H. Zhang, H. Shi, K. Konynenbelt, H. Luo, and Y. Liu, "Over 5-W passively Q-switched mid-infrared fiber laser with a wide continuous wavelength," IEEE Photon. Technol. Lett. **29**, 881–884 (2017).
18. S. G. Ning, G. Y. Feng, H. Zhang, W. Zhang, S. Y. Dai, Y. Xiao, W. Li, X. X. Chen, and S. H. Zhou, "Fabrication of Fe^{2+}:ZnSe nanocrystals and application for a passively Q-switched fiber laser," Opt. Mater. Express **8**, 865–874 (2018).
19. C. Wei, X. S. Zhu, F. Wang, Y. Xu, K. Balakrishnan, F. Song, R. A. Norwood, and N. Peyghambarian, "Graphene Q-switched 2.78 μm Er^{3+}-doped fluoride fiber laser," Opt. Lett. **38**, 3233–3235 (2013).
20. J. F. Li, H. Y. Luo, L. L. Wang, C. J. Zhao, H. Zhang, H. P. Li, and Y. Liu, "3-μm mid-infrared pulse generation using topological insulator as the saturable absorber," Opt. Lett. **40**, 3659–3662 (2015).
21. C. Wei, H. Y. Luo, H. Zhang, C. Li, J. T. Xie, J. F. Li, and Y. Liu, "Passively Q-switched mid-infrared fluoride fiber laser around 3 μm using a tungsten disulfide (WS_2) saturable absorber," Laser Phys. Lett. **13**, 105108 (2016).
22. P. H. Tang, Y. Tao, Y. L. Mao, M. Wu, Z. Y. Huang, S. N. Liang, X. H. Chen, X. Qi, B. Huang, J. Liu, and C. J. Zhao, "Graphene/MoS_2 heterostructure: a robust mid-infrared optical modulator for Er^{3+}-doped ZBLAN fiber laser, " Chin. Opt. Lett. **16**, 020012 (2018).
23. Z. P. Qin, G. Q. Xie, H. Zhang, C. J. Zhao, P. Yuan, S. C. Wen, and L. J. Qian, "Black phosphorus as saturable absorber for the Q-switched Er:ZBLAN fiber laser at 2.8 μm," Opt. Express **23**, 24713–24718 (2015).
24. J. F. Li, H. Y. Luo, B. Zhai, R. G. Lu, Z. N. Guo, H. Zhang, and Y. Liu, "Black phosphorus: a two-dimension saturable absorption material for mid-infrared Q-switched and mode-locked fiber lasers," Sci. Rep. **6**, 30361 (2016).
25. K. S. Novoselov, A. K. Geim, S. V. Morozov, D. Jiang, Y. Zhang, S. V. Dubonos, I. V. Grigorieva, and A. A. Firsov, "Electric field effect in atomically thin carbon films," Science **306**, 666–669 (2004).
26. Q. L. Bao, H. Zhang, Y. Wang, Z. Ni, Y. Yan, Z. Shen, K. P. Loh, and D. Y. Tang, "Atomic-layer graphene as saturable absorber for ultrafast pulsed laser," Adv. Funct. Mater. **19**, 3077–3083 (2009).
27. V. Tran, R. Soklaski, Y. Liang, and L. Yang, "Layer-controlled band gap and anisotropic excitons in few-layer black phosphorus," Phys. Rev. B **89**, 235319 (2014).
28. Y. F. Song, Z. M. Liang, X. T. Jiang, Y. X. Chen, Z. J. Li, L. Lu, Y. Q. Ge, K. Wang, J. L. Zheng, S. B. Lu, J. H. Ji, and H. Zhang, "Few-layer antimonene decorated microfiber: ultra-short pulse generation and all-optical thresholding with enhanced long term stability," 2D Mater. **4**, 045010 (2017).
29. G. Wang, R. Pandey, and S. P. Kama, "Atomically thin group V elemental films: theoretical investigations of antimonene allotropes," ACS Appl. Mater. Interfaces **7**, 11490–11496 (2015).
30. S. Zhang, M. Xie, F. Li, Z. Yan, Y. Li, E. Kan, W. Liu, Z. Chen, and H. Zeng, "Semiconducting group 15 monolayers: a broad range of band gaps and high carrier mobilities," Angew. Chem. **128**, 1698–1701 (2016).
31. S. K. Gupta, Y. Sonvane, G. X. Wang, and P. Ravindra, "Size and edge roughness effects on thermal conductivity of pristine antimonene allotropes," Chem. Phys. Lett. **641**, 169–172 (2015).
32. S. Zhang, Z. Yan, Y. Li, Z. Chen, and H. Zeng, "Atomically thin arsenene and antimonene: semimetal-semiconductor and indirect-direct band-gap transitions," Angew. Chem. **127**, 3155–3158 (2015).
33. M. Zhao, X. Zhang, and L. Li, "Strain-driven band inversion and topological aspects in antimonene," Sci. Rep. **5**, 16108 (2015).
34. Y. F. Xu, B. Peng, H. Zhang, H. Z. Shao, R. J. Zhang, and H. Y. Zhu, "First-principle calculations of phononic, electronic and optical properties of monolayer arsenene and antimonene allotropes," Ann. Phys. **529**, 1600152 (2017).
35. M. X. Wang, F. Zhang, Z. P. Wang, Z. X. Wu, and X. G. Xu, "Passively Q-switched Nd^{3+} solid-state lasers with antimonene as saturable absorber," Opt. Express **26**, 4085–4095 (2018).
36. J. P. Ji, X. F. Song, J. Z. Liu, Z. Yan, C. X. Huo, S. L. Zhang, M. Su, L. Liao, W. H. Wang, Z. H. Ni, Y. F. Hao, and H. B. Zeng, "Two-dimensional antimonene single crystals grown by van der Waals epitaxy," Nat. Commun. **7**, 13352 (2016).
37. J. Zhang, D. H. Li, R. J. Chen, and Q. H. Xiong, "Laser cooling of a semiconductor by 40 kelvin," Nature **493**, 504–508 (2013).
38. D. H. Li, J. Zhang, and Q. H. Xiong, "Laser cooling of CdS nanobelts: thickness matters," Opt. Express **21**, 19302–19310 (2013).
39. L. Lu, X. Tang, R. Cao, L. M. Wu, Z. J. Li, G. H. Jing, B. Q. Dong, S. B. Lu, Y. Li, Y. J. Xiang, J. Q. Li, D. Y. Fan, and H. Zhang, "Broadband nonlinear optical response in few-layer antimonene and antimonene quantum dots: a promising optical Kerr media with enhanced stability," Adv. Opt. Mater. **5**, 1700301 (2017).
40. C. H. Zhu, F. Q. Wang, Y. F. Meng, X. Yuan, F. X. Xiu, H. Y. Luo, Y. Z. Wang, J. F. Li, X. J. Lv, L. He, Y. B. Xu, J. F. Liu, C. Zhang, Y. Shi, R. Zhang, and S. N. Zhu, "A robust and tuneable mid-infrared optical switch enabled by bulk Dirac fermions," Nat. Commun. **8**, 14111 (2017).
41. B. Braun, F. X. Kärtner, G. Zhang, M. Moser, and U. Keller, "56-ps passively Q-switched diode-pumped microchip laser," Opt. Lett. **22**, 381–383 (1997).
42. C. Hönninger, R. Paschotta, F. Morier-Genoud, M. Moser, and U. Keller, "Q-switching stability limits of continuous-wave passive mode locking," J. Opt. Soc. Am. B **16**, 46–56 (1999).